ACS APPLIED MATERIALS & INTERFACES

Research Article

www.acsami.org

Band Alignment in Partial and Complete ZnO/ZnS/CdS/CuSCN Extremely Thin Absorber Cells: An X-ray Photoelectron Spectroscopy Study

Eran Edri,[†] Hagai Cohen,[‡] and Gary Hodes*[,†]

[†]Department of Materials and Interfaces and [‡]Department of Chemical Research Support, Weizmann Institute of Science, Rehovot 76100, Israel

Supporting Information

ABSTRACT: In all solar cells, and especially in extremely thin absorber (ETA) solar cells, proper energy band alignment is crucial for efficient photovoltaic conversion. However, available tabulated data usually do not agree with actual results, and in most cases, V_{oc} values lower than expected are achieved. In fact, ETA cells suffer from a very low V_{oc}/E_{gap} ratio, such as in ZnO/CdS/CuSCN cells. Here, we investigate limiting factors of ZnO/CdS/CuSCN ETA cells, applying X-ray photoelectron spectroscopy (XPS), chemically resolved electrical measurement (CREM), Kelvin probe, and $I-V$ characterization. We show that electric fields are gradually developed in the cell upon increased absorber thickness. Moreover, an accumulation layer, unfavorable for the solar cell function, has been revealed at the oxide−absorber interface An effective chemical treatment to prevent formation of this accumulation layer is demonstrated.

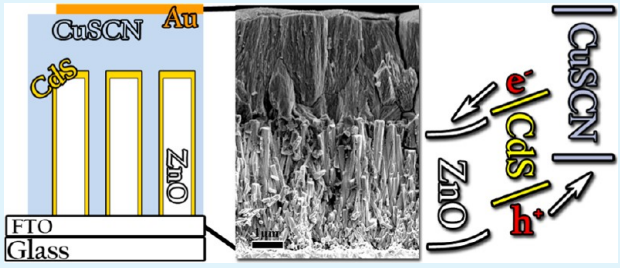

KEYWORDS: *ETA cells, semiconductor-sensitized, band diagram, CREM, V_{oc} limit, LiSCN*

INTRODUCTION

Knowledge of energy band diagrams in electronic devices in general and photovoltaic cells in particular is clearly very important for understanding and improving their performance. In extremely thin absorber solar cells (ETA cells), photon absorption and charge transport processes take place, for the most part, in different material phases (absorption in the absorber and transport mainly in the electron and hole conducting phases). By using a porous structure for the cell, the local absorber thickness can be reduced to typically some tens of nanometers, yet maintaining a high overall optical thickness to absorb all or most of the relevant light. Thus, the distance a charge needs to travel to the interface is reduced, which reduces the chance for recombination in the absorber.[1,2]

In ETA cells, if a band picture is given, it is most often based on literature values of the isolated phases and using the Anderson model (electron affinity rule) for band alignment. Such a method has a number of serious deficiencies: The often wide range of values of electron affinities in the literature; the common failure of the electron affinity rule[3] and, particularly important, the interaction between the various phases, when several different materials are sequentially deposited, is neglected.

X-ray photoelectron spectroscopy (XPS) and UV photoelectron spectroscopy (UPS) are commonly used to map energy band diagrams of solar cells in general. While UPS enables energy resolution higher than XPS, it cannot, in most cases, monitor the core level energies of buried layers, both because of the relatively low energy of the UV radiation as well as the extreme surface specificity of UPS. XPS can access all core levels and is somewhat less limited in depth compared to UPS.

The fact that at least three different materials are assembled together in an ETA cell, together with its porous structure (which is beneficial for strong light absorption), makes determination of the band diagram more demanding than for conventional cells. At the same time, we have shown that this morphology can also be advantageous for XPS + CREM (chemically resolved electrical measurement)[4] analysis of ETA cells insofar as it allows the XPS probe to "see" deep into the cell.[5] The importance of this ability is that, by analyzing the core levels of the elements in the cell as it is built up one "layer" at a time, changes, both chemical and electrical, that might occur in underlying layers due to deposition of subsequent layers (even beyond the one immediately following) can be detected.

ETA cells are mostly made using either TiO_2 nanoparticles or ZnO nanorods as electron conductors. The two different materials and morphologies lead to important differences in the resulting cells for two major reasons. One is the more regular and usually more open structure of the ZnO nanorods, which allows easier access to all oxide domains (for both absorber and

Received: March 19, 2013
Accepted: May 16, 2013
Published: May 16, 2013

hole conductor deposition). A second, and possibly more important reason, is that deposition of absorbers, usually sulfides or selenides, on TiO_2 generally leads to isolated island growth, whereas growth on ZnO can be (though not always) in the form of a reasonably coherent layer covering the entire ZnO surface. The morphology of absorber coating on ZnO depends on the method of deposition. This can be traced to the formation of a thin ZnS layer on the more chemically reactive ZnO (than TiO_2) substrate, either intentionally or during deposition. Solar cells with island growth have been found to be considerably poorer than those with a uniform growth.[6]

The absorber morphology on the oxide is certainly important for the cell mechanism (there is more likely to be an electric field across a coherent absorber layer than if the absorber is in the form of isolated islands). It is also important in the context of XPS-based energy band structure measurements since a coherent absorber layer reduces the ability to probe the underlying oxide. However, having usually no more than a few tens of nm of the absorber thickness, means that a weak oxide signal (enough for our needs) may still be seen.

Our main goal in this study is to map the energy band diagrams of ZnO nanorod-based ETA cells using XPS/CREM so as to find out not just the band offsets that are so important in ETA cells but also the built-in electric fields in the cells, their existence, magnitude, and direction. These are all important questions to understanding and eventually improving the device efficiency. For this purpose, we investigate the ZnO\CdS \CuSCN ETA cell and, in addition, look at the effect on band structure of LiSCN solution treatment in an attempt to understand better its role.

1. EXPERIMENTAL SECTION

Fluorine-doped tin oxide (FTO, 8Ω/□) slides were cut to 1.2 cm × 4.5 cm and cleaned by sonication for 15 min each in acetone, methanol, warm Alconox (60−70 °C; 1 g/100 mL), and warm water and rinsed well with deionized water (Millipore 18 Ω·cm).

ZnO was deposited in a three-step procedure. First the substrate was activated by seeding with MnO_x crystallites as was described elsewhere.[7] In short, each slide was placed in a preheated bath for 30 min at 90 °C in a 0.5 mM $KMnO_4$ (Fluka) aqueous solution with a few drops of *n*-butanol (Merck) as a mild reducing agent. The slides were thoroughly washed with water, sonicated for 5 min, and then rinsed again before being transferred to the first ZnO chemical bath for deposition of the dense ZnO layer. For the dense layer, the composition of the aqueous bath was: 0.1 M Zn acetate, 1 mM Sb tartrate ($KSbO{\cdot}C_4H_4O_6$), 1.67 M ethanolamine, and 0.4 M ammonia (all Merck, high purity chemicals). The bath was heated to 90 °C for 10 min. The samples were then quickly rinsed with deionized water and transferred to the second ZnO bath for deposition of the ZnO nanorods. The composition of this second bath was like the first, only without the Sb salt and with 0.8 M (instead of 0.4 M) ammonia. Deposition was carried out at 90 °C for 30 min followed by drying with a N_2 stream.

Prior to absorber deposition, the slides were annealed in air at 350 °C for 2 h. For uniform coating of the ZnO rods by the CdS, a thin surface layer of ZnS was formed by chemical exchange (treatment in 0.1 M aqueous Na_2S (Sigma-Aldrich) solution for 5 min).[6] The slides were again rinsed thoroughly in water and then immersed in the CdS chemical bath (0.025 M Cd acetate (Sigma-Aldrich), 0.1 M ethylenediamine, 0.1 M thiourea). Deposition was carried out at room temperature in the dark for times specified in the text. The slides were rinsed with water and dried in a N_2 stream. For all the solution processes above, the slides were placed tilted at ∼30° with the FTO side facing downward to prevent bulk precipitation on this face.

For the thiocyanate treatment, when used, the CdS-covered ZnO was dipped in a 0.5 M solution of the thiocyanate of the chosen cation (Li^+, Na^+, K^+, NH_4^+, guanidinium) for 5 min at room temperature and then wick-dried with Kimwipe tissue.[8] CuSCN (Sigma-Aldrich) was deposited from a nearly saturated (slightly diluted 1:1.08) di-*n*-propyl sulfide (Alfa Aesar) solution through a 90° bent needle closed at the end, with four holes at the lower side following a method described elsewhere.[9] The solution was pumped through the holes from a syringe pump at a rate of 18 μL/min. The slide was put on a heated plate at 62 °C. 0.18 mL/cm^2 of the CuSCN solution was used, which fills the pores and also forms at least 1 μm of CuSCN on top of the ZnO rods.

To complete the cells, a gold back contact (80 nm thick) was evaporated (Edwards e-beam) onto the CuSCN. The cell area to be measured was scribed (not less than 1 cm^2) and masked with an aperture the same area as the scribed sample area.

Samples for transmission electron microscopy (TEM) were prepared by scratching a part of the film, sonicating it in methanol for a few minutes, and then spreading the solution on a Cu TEM grid with a carbon layer. Images were taken on a FEI CM-120 microscope equipped with a CCD camera. Scanning electron microscopy (SEM) images were taken on a Zeiss ULTRA or SUPRA high resolution microscope. No special preparation procedures were taken, except with the cross section images, where the sample was cleaved just before putting it into the high vacuum chamber.

To measure the current−voltage characteristics, the cell was put in a sealed dark-box with an appropriate mask. The *I*−*V* was measured with a Keithley 2400-LV SourceMeter and controlled with a Labview-based, in-house designed program. A solar simulator (ScienceTech SF-150) calibrated with a Si solar cell IXOLAR High Efficiency SolarBIT (IXYS XOB17-04 × 3) was used for illumination.

X-ray photoemission spectroscopy (XPS) was carried out on a Kratos AXIS ULTRA-DLD system, using a monochromatic Al (Kα) X-ray source ($h\nu$ = 1486.6 eV) at 75 W and detection pass energies between 10 and 80 eV. For the CREM electrical loops, either the eFG (flood gun) bias, or the sample bias was varied while XPS measurements were taken. The changes in peak positions were thus monitored and, simultaneously, the current through the sample was measured. For light induced CREM a halogen light source (with no UV component) was used. Extraction of the surface potential using CREM is described elsewhere,[10] The XPS-derived average thickness values of the ZnS layer were calculated by using the following expression (suited for a planar, uniform coating):

$$d = \lambda \ln(1 + I_{ZnS}/I_{ZnO})$$

Where d is the thickness of the ZnS layer, λ is the photoelectron inelastic mean free path (chosen to be 2.5 nm), and I_{ZnS} and I_{ZnO} are the intensities measured for ZnS and ZnO, respectively.

Contact potential difference (CPD) was measured with an in-house built Kelvin probe setup based on a commercial Besocke Delta Phi Kelvin probe and controller. All samples were measured in a controlled atmosphere box with <10% relative humidity. The surface potential was measured relative to that of a vibrating Au grid (5 mm diameter), whose work function (WF) was determined to be 4.75 eV by comparing to a standard of a freshly cleaved highly oriented pyrolytic graphite with a nominal work function of 4.6 eV. Once a connection was made and a good signal was acquired, the samples were allowed to equilibrate and only then a measurement of the CPD was taken. For surface photovoltage (SPV) measurements, to avoid heating of the sample, a digitally controlled cool white LED lamp was used as a light source; the light intensity of the LED was calibrated with a photodiode and normalized (only the linear part of the LED response was used; maximum light intensity is estimated as 25 mW/cm^2). After each change of the light intensity, the sample was allowed to equilibrate before a measurement was taken. Each measurement is given as an average of several separate regions of a number of different samples.

XPS/CREM/"Electrical Loops" Methodology. As noted above, using the electron affinity rule to estimate band alignments presents problems, one of which is energy level shifts due to interactions between phases. A partial answer to this problem was provided by Kraut,[11,12] who used XPS core levels as a reference for corresponding valence band (VB) edges of the materials. By comparing "free

standing" films of the individual materials with a combined system (with a thin "enough" overlayer), the VB edge offset between materials A and B, ΔE_V, could be obtained:

$$\Delta E_V = (E_{CL}^A - E_{CL}^B)|_{thin} + (E_{CL}^B - E_{VBM}^B)|_{thick} - (E_{CL}^A - E_{VBM}^A)|_{thick} \quad (1)$$

where E_{CL} and E_V refer to the energies of the core level and valence band edge, respectively, of the relevant material. In the first term, both values are taken from a sample with a thin overlayer.

Recently, a more consistent XPS-based approach was demonstrated, with a better elimination of probe-induced changes in the electrostatic potential, as inspected at the various domains and, importantly, with in situ follow−up of the work-function (WF) changes.[5] This latter approach is applied here, including exposure to elevated electrical stimuli (see the electrical loops described next) with which the dielectric properties of the system can be studied layer by layer, while monitoring the "buried" layers.

As demonstrated in the past,[4,5] an important outcome of monitoring the core level energies is that spontaneous and induced electrostatic potentials evolving in the sample can be evaluated and done so for each separate element. Evaluation of the respective charging is done by irradiating the sample with an electron flood gun (eFG) with controlled energy and flux, in addition to the X-ray photoemission process, while monitoring the core level peak energy shifts and also the current passing through the sample. In a simplistic picture, when the eFG electrons are emitted with insufficient energy to reach the surface (alternatively, when the sample is held at a relatively large forward bias), the sample is affected by the X-ray irradiation only, with typically small (<1 nA) sample current. Once enough energy is provided to the eFG electrons so that they do reach the sample surface (or alternatively the sample bias is reduced), electrons can (ideally) neutralize the charging caused by X-ray photoemission and further induce negative charging. If the electron energy is further increased, the electrical current through the sample (with an opposite direction to the small current initially measured) increases. Under these conditions, large shifts in peak positions are expected. Through this experiment, two goals are achieved: First, the accuracy of the band position measurement is improved, as corrections for the initial X-ray induced charging can be made. The importance of this correction is amplified when the charging is not uniform across the morphologically complex multilayer. Second, by following the induced changes in peak energies of elements representative of the multilayered structure, one can reveal important information on the tendency of specific layers and interfaces to trap positive or negative charge.

A small signal from the ZnO was detected even for relatively thick overlying layers. This was possible due to small voids in the overlayer, as already described by us for TiO_2-based cells[5] (these voids occur to a lesser extent in ZnO-based cells, reflecting better coverage of the ZnO/ZnS surface). Measuring the ZnO through voids in the CdS and/or CuSCN coating, a question may be raised on the relevance of corresponding electrostatic potential values to those interfaces underneath the CdS particles. As already noted,[5] with a screening length sufficiently large compared to the size of these voids (a limit even better fulfilled by the present system), the detected potentials should indeed represent reliably the relevant CdS/ZnO interfaces.

RESULTS

The results section is divided such that each interface is analyzed separately in the order of the cell fabrication. In each case the VB offset is calculated from the core level peak positions, and then corrections due to charging (if required) are applied.

A. Energy Bands Alignment from Partial and Complete Cells. *1. ZnO\\ZnS Interface.* The outer layer of the ZnO rods is converted to ZnS by dipping in Na_2S solution at room temperature, the thickness being controlled by the duration of the dip. This layer promotes uniform growth of the absorber. From XPS and TEM studies, we found that a 5 min dip results in an average ZnS thickness of 0.8−1 nm on the ZnO. A 110 min dip results in an average thickness of ca. 10 nm (ca. 2 layers of <5 nm particles, Figure 1).

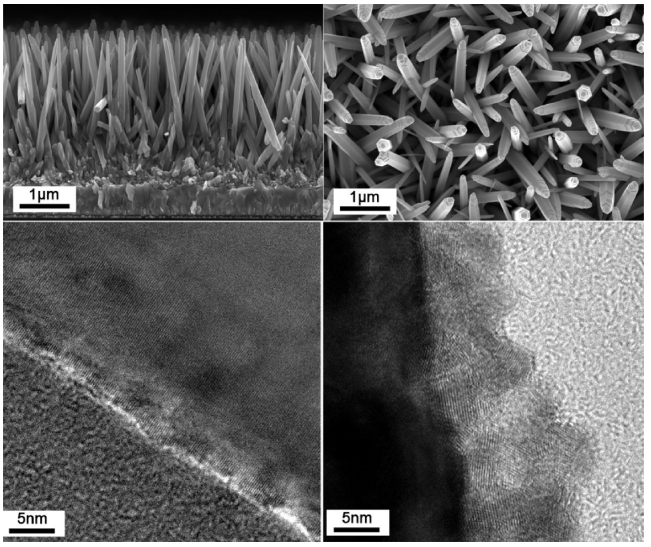

Figure 1. (upper) Cross-section and plan views of ZnO films, rod length of ∼2.5 μm and rod diameter of ∼200 nm. (lower left) Thin (5 min dip) ZnS on ZnO; average thickness of 0.8 nm was measured by XPS. (lower right) Thick ZnS on ZnO (110 min dip; typically ca. 10 nm).

Since the ZnO and ZnS phases are not resolved in the XPS Zn2p peak, the S2p and O1s lines were chosen for band offset evaluation. The resultant VB edge offset is −1.0 ± 0.1 eV, in agreement with theoretical calculations,[13,14] and previous experimental measurements.[14] Direct comparison of the VB edge in bare-ZnO and ZnO with thin ZnS reveals a 1.0 eV difference, with additional states added at the top of the ZnO VB. These additional states are attributed to the ZnS VB edge.

Figure 2 compares the O and S peak positions in ZnO, ZnO/ZnS(thin), and ZnO/ZnS(thick). After formation of thin ZnS, the Zn2p peak is not shifted, while the O1s is shifted by 0.14 eV to lower binding energy (BE). Also, the WF does not change in going from ZnO to ZnO/ZnS(thin). Between thin and thick

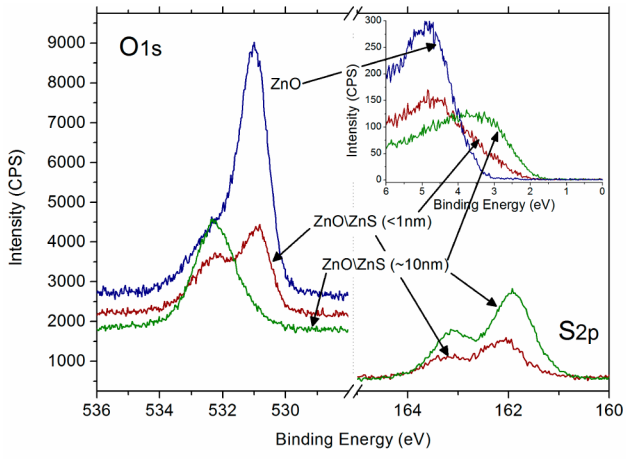

Figure 2. O1s, S2p, and VB edge (inset) spectra of ZnO (blue), thin ZnS on ZnO (brown), and thick ZnS on ZnO (green).

dx.doi.org/10.1021/am401010f | ACS Appl. Mater. Interfaces 2013, 5, 5156−5164

ZnS, the S2p BE is shifted by −0.15 eV while Zn2p is shifted by −0.03 eV (not shown) and the corresponding O1s peak by −0.05 eV for thick ZnS layers. The WF of ZnO measured in vacuum by CREM is 4.05 ± 0.05 eV, while with a Kelvin probe (KP) in dry N_2 environment, we obtain 4.35 ± 0.1 eV. This difference can be attributed to the different environment (comparing the methods on test samples yields agreement within 100 meV). When ZnS is formed on ZnO, no significant change, by either method, is observed in the WF, as long as the ZnS layer is thin. For thick ZnS layers, the WF measured by CREM increases by 200 meV compared to ZnO (a 50 meV increase measured by KP). Changes in WF upon deposition of ZnS on ZnO were reported by others (up to 1.7 eV increase in WF)[15] and were attributed to a dipole created at the interface plus band bending in the ZnO. However different preparation methods of ZnO lead to different WF values (values ranging between 3.7 and 6 eV),[15] possibly due to differences in surface composition, crystal faces, and effective doping levels.

Both the core level shift and WF increase when increasing the ZnS thickness could be an outcome of better surface coverage (ZnS on ZnO) while creating a built-in field (either in the ZnO and/or the ZnS). We do not consider this case further since we do not use the thick ZnS layer in our cells.

During photoelectron measurements, semiconducting samples frequently accumulate charge as a result of the electron emission. In multilayered structures, differential charging frequently evolves, with different magnitudes at each of the layers. We would like to eliminate these beam-induced effects and we do it by monitoring representative signals of each layer and follow their spectral shifts under varying electrical stimuli, i.e. those induced by the eFG. The first sample we examine this way is ZnO and ZnO/ZnS(thin) (Figure 3).

No shift in the Zn2p or O1s peak position is found when V_G (the eFG, bias voltage) is increased up to 3.55 V. At higher values, the current through the sample increases and the peak begins to shift almost linearly with applied voltage. When V_G is gradually reduced to its original value, no hysteresis is observed. This behavior (lack of hysteresis and no peak shifts in the early part of the scan) indicates no significant charging in the ZnO; namely, the layer can efficiently evacuate any externally induced residual charge. This is reasonable for our ZnO with high mobility and carrier density on the order of 10^{17} cm^{-3} (as deduced from the measured Fermi level position). The irreversibility (hysteresis) observed for C1s reflects a chemical change that takes place during the process (including loss of carboxylate groups adsorbed at the surface, as indicated by the changes in shape of the C1s and O1s peaks under radiation; not shown). The O-curve hysteresis is smaller, but generally consistent with that of the C-curve.

This picture slightly changes when a thin layer of ZnS is deposited on the surface. Taking the S2p as a representative element of the ZnS and the O1s for the ZnO, the negative ΔE_K of S2p (a shift to smaller E_K during V_G steps before the eFG electrons can reach the surface) indicates positive charging of the ZnS. The magnitude of this effect is not large, ca. 50 meV, but it is reproducible. At the same time, some positive ΔE_K may be noted at the O1s peak. Thus, in this structure, the ZnS exhibits a tendency to capture holes, presumably attracted from the ZnO substrate.

2. ZnO\ZnS\\CdS. As a result of the sulfide treatment, CdS is deposited uniformly on ZnO (with a thin—0.8 nm—layer of ZnS), as a layer of nanoparticles, 4−5 nm in diameter. The CdS thickness is controlled via deposition time. Three CdS

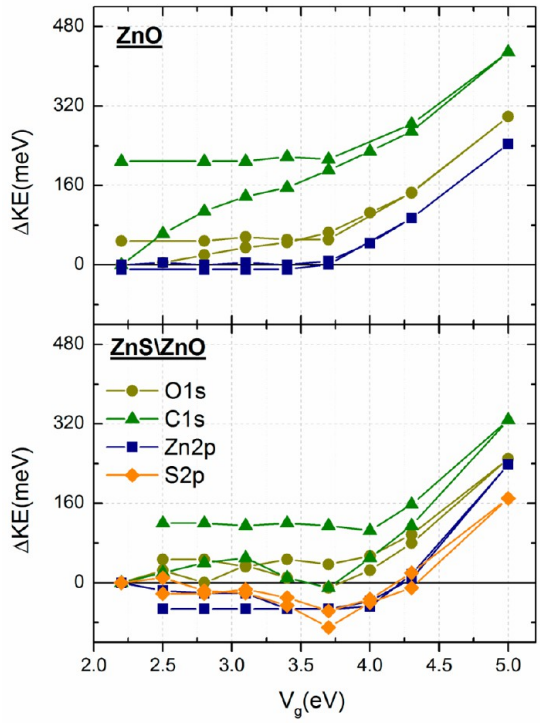

Figure 3. Electrical loops: Shifts in peak positions of ZnO (top) and ZnS/ZnO (bottom) under varying electrical stimuli. The sample bias is kept constant while the eFG bias is varied. Elements shown: Zn2p (squares), O1s (circles), S2p (diamonds), and C1s (triangles). The ΔE_K scale for all curves refers to the initial measurement of each element.

thicknesses were examined: thin (5−10 nm), medium (10−15 nm), and thick (20−30 nm). Thicknesses were estimated from TEM images (Supporting Information Figure S1).

Following the method described above, the VB offset of CdS relative to ZnS was calculated to be −0.1 ± 0.1 eV. The Cd3d and Zn2p peaks were used for these calculations (again, the Zn2p peak showed no significant BE difference between ZnO and thin ZnS). The total band offset between ZnO and CdS is in agreement with previously calculated and measured values,[16,17] and is virtually unaffected by the ZnS layer.

Interestingly, while the Zn2p peak position in ZnO and ZnO\ZnS is the same, deposition of a thin CdS layer shifts the Zn2p peak by 200 meV to lower E_K (Figures 4 and 5). Further increase in CdS thickness shifts the Zn2p peak by an additional 150 meV (Figure 5, green line) and eventually, it saturates for CdS thickness of 20−30 nm. In contrast, the Cd3d and S2p peaks shift by 300 meV to higher E_K upon increasing CdS thickness, from 5 to 10 nm to 10 to 15 nm, with no further change for CdS thickness of 20−30 nm. Accordingly, the CREM-derived WF of these ZnO\ZnS\CdS films increases by 100 meV upon initial CdS deposition up to 10−15 nm and, then, decreases by 100 meV for the thick CdS layer (20−30 nm). The KP WFs show the same tendencies, but with systematically larger values, ca. 50−350 meV (depending on the sample; Figure 5).

The E_K increase in Zn2p after CdS deposition indicates that the energy levels of ZnO shifted downward, reflecting a field created in the ZnO. This could be either formation of an accumulation layer or a reduction of an original depletion layer as a consequence of the CdS deposition. Importantly, when the CdS thickness is increased, the Zn2p and Cd3d peaks shift in

dx.doi.org/10.1021/am401010f | ACS Appl. Mater. Interfaces 2013, 5, 5156−5164

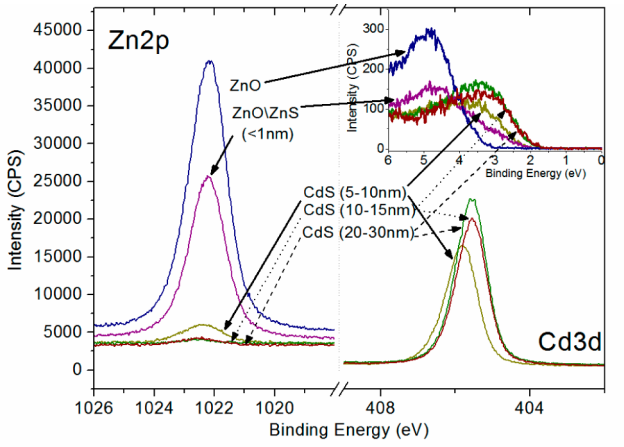

Figure 4. Zn2p and VB edge spectra of ZnO and ZnO\thin ZnS (blue; purple); Cd3d, Zn2p, and VB spectra of thick, medium, and thin (green, red, and yellow, respectively) of CdS on ZnO\thin ZnS.

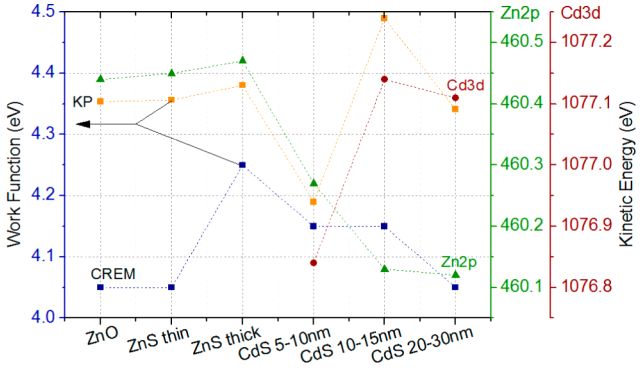

Figure 5. Sample energetics under sequential deposition steps: Work function (measured with CREM (blue squares) and KP (orange squares)). Zn2p (green triangles) and Cd3d (brown circles) peak positions. CdS was deposited on thin ZnS. Lines connecting points are only guidelines to the eye.

opposite directions (to lower and higher E_K, respectively) until a constant value is reached for both lines.

Considering the process as an n−n heterojunction formation, the difference in WF, ZnO, vs CdS-on-ZnO is not large (<0.1 eV at most). The ZnO E_K change (decrease) is more significant (0.25−0.35 eV, depending on CdS thickness). Therefore the WF change is insufficient to explain this effect. The E_K increase in ZnO reflects a field created in the ZnO bulk *or* at the very surface. The latter is unlikely since the Zn-peak shifts continuously with increasing CdS thickness (up to 10−15 nm). Extremely thin CdS—ca. 1 nm—tested in a separate experiment (not shown), shows only a small Zn2p E_K shift, <100 meV, and an even smaller Cd3d shift (50 meV) between bare ZnO and ca. 5 nm CdS coating, implying no (or a very small) dipole creation during initial CdS deposition. The accumulation field (or reduction field in depletion) in the ZnO could form traps for electrons transferred to the ZnO, resulting in a poorer removal of extra electrons from the ZnO surface. The Cd3p E_K increase for thicker CdS implies a depletion field (CB slanting from the CdS surface down toward the ZnO), which evolves with the CdS thickness. This field direction promotes electron injection into the ZnO, especially electrons generated away from the ZnO/CdS interface.

Monitoring the charging in the layers (Supporting Information Figure S2) we find that for both the thin and the thick CdS films, the Zn2p peak exhibits either a small (thick CdS) or no (thin CdS) shift to higher E_K over time, indicating a small degree of positive charging (it should be noted that the Zn2p signal in the thick CdS sample is small and noisy and the experimental error is therefore large). On the other hand the Cd3d (and S2p) peaks shift to lower E_K which indicates negative charging. In the intermediate thickness sample, all peaks seem to shift in the same direction and in the same order of magnitude. The C1s shifts indicate that carbon is going through a chemical change during the process (much more significant in the intermediate-thickness sample), similar to the ZnO sample. To conclude, the representative peaks seem to shift by ∼100 meV after long and intensive radiation (the Cd3d significantly more than the Zn2p), which indicates that the CdS layer tends to capture electrons.

3. ZnO\ZnS\CdS\\CuSCN. A complete ETA solar cell (Figure 6) is made by depositing a hole conductor into the

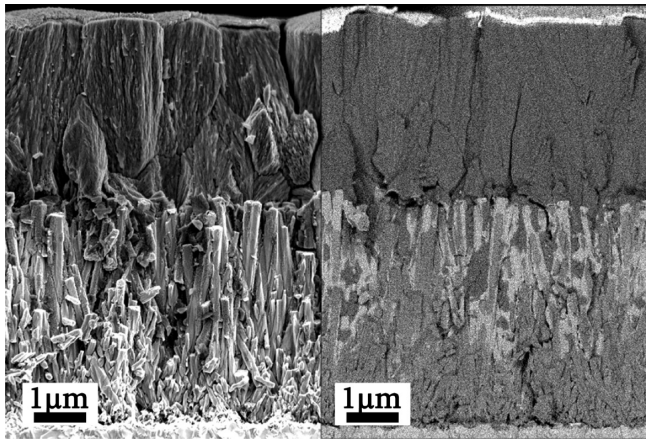

Figure 6. SEM image of a cross section of a complete ZnO\CdS \CuSCN ETA solar cell. The image is equally divided into an InLens detector image (left-hand side) which is sensitive to the morphology and back scattered electron detector (right-hand side), which is more sensitive to the atomic number (heavier elements appear lighter). The scale bar is 1 μm.

pores of the meso-structured substrate. A layer of ca. 2 μm is deposited (on top of the ZnO rods) to separate the rods from the back contact.

This part of the investigation is carried out on CdS of ca. 15 nm thick as this thickness showed the highest solar cell efficiency. Our examination of the energy structure across the CdS/CuSCN interface is divided into two cases: with and without a thiocyanate treatment. The thiocyanate treatment is known to improve the solar cell performance (ca. 100% improvement in V_{oc}), but the reason for this improvement is not yet clear.[8]

First we consider the band structure without the LiSCN treatment. Following the methodology used for the other interfaces above, we find that for the ZnO\ZnS\CdS\CuSCN structure, the CuSCN VB is positioned 1.2 ± 0.1 eV above that of the CdS; a value derived from the Cu2p and Cd3d peaks.

Figure 7 shows changes in WF and core level peak positions as each component of the cell is added. For the nontreated sample, initial deposition of CuSCN on the substrate increases the WF by 0.70 eV to 4.85 ± 0.05 eV. For the full CuSCN thickness, the WF does not change further (i.e., a little CuSCN

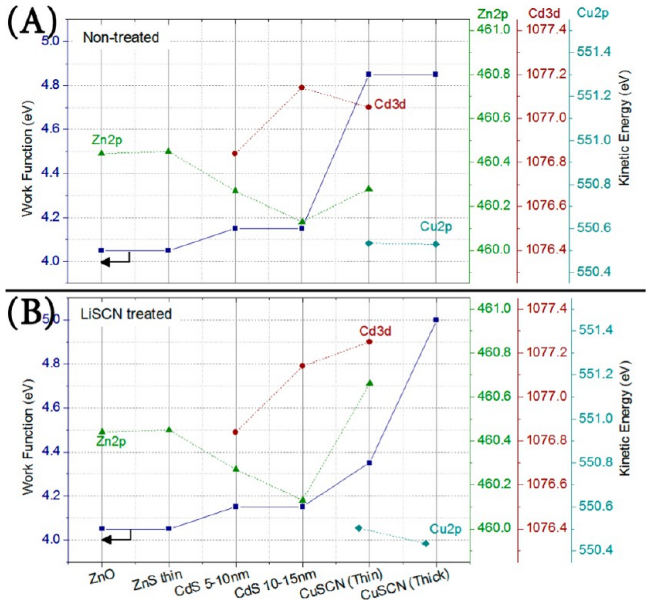

Figure 7. Variation of work function and core level peak positions under successive steps in solar cell build-up. (A) Nontreated. (B) Thiocyanate treated. Thin CuSCN refers to ca. 7% of the total CuSCN deposited; thick refers to a complete cell, with an overlayer of 1−2 μm. Lines connecting points are only guidelines to the eye.

is sufficient to reach the final WF). For thin CuSCN, the Cd3d peak shifts to lower E_K by 0.10 eV and the Zn2p peak shifts *in the opposite direction* to higher E_K by 0.15 eV for thin CuSCN. We could not measure the Zn and Cd core levels after deposition of the thick CuSCN; however the fact that neither the Cu2p peak position nor the WF is changed when going from thin to thick CuSCN suggests that the underlying core levels may not change either (with the reservation that under nonuniform initial coverage, such changes may take place).

For the sample treated with an aqueous solution of LiSCN prior to the CuSCN deposition, we inspected the system with a thin CuSCN layer. The Zn2p peak shifted to higher E_K by 0.55 eV and the Cd3d by 0.11 eV *in the same direction*. The Cu2p E_K decreased by 0.05 eV from the thin to thick CuSCN while the WF increased first by 0.20 eV (thin CuSCN) and by a further 0.65 to 5.0 eV for a thick layer of CuSCN, a total increase of 0.85 eV. For comparison, the WF of CuSCN deposited directly onto a FTO substrate (measured by CREM) is 4.9 ± 0.05 eV.

To summarize, and provided that no chemical changes interfere, the observed line shifts represent electrostatic potential changes. The much greater shift of Zn2p to higher E_K for the treated sample suggests stronger depletion at the ZnS/ZnO region, compared to the untreated sample. This would involve electron injection into the ZnO rods, keeping the charge away from the surface, thus reducing electron−hole recombination across the interface of ZnO with any of the other phases.

The higher E_K of Cd3d for treated samples suggests a greater internal field in the CdS of a treated cell, which should act to improve separation of electrons and holes within the CdS itself. And finally, the small, yet observable, 50 meV increase in Cu2p energy may indicate higher doping at the CuSCN near its interface with the CdS, as a result of the thiocyanate treatment.

Electrical loops were carried out for treated and nontreated samples and for both thin and thick CuSCN—a total of 4 samples (Supporting Information Figure S3). In all cases, charging in the CuSCN was found to be small, appearing after long exposures to high eFG flux. The Cu2p signal exhibits hysteresis typical of negative charging at magnitudes that are sample dependent. Hysteresis of the opposite sign, as compared to the Cu2p line, is found in the S2p signal (also C1s and N1s) and is particularly noticeable for the thick, treated sample. We attribute this to a chemical change, i.e. a different ionicity between the Cu^+ and the SCN^-. At the same time, other elemental signals show different trends, depending on the prior treatment. In a treated thin sample, all peaks exhibit a shift of common sign, with roughly the same magnitude (the S2p slightly more than the others), indicating opposite charging with respect to the Cu2p. In contrast, the thin sample without LiSCN shows a different charging pattern—the hysteresis in the Zn2p signal may indicate that negative charge is trapped in the ZnO. This finding supports our previous notion of negative charge accumulation in the ZnO\CdS interface, extracted from the "stepwise peak shift" analysis presented above. This also shows the importance of the electrical loop method in investigating domain-specific charging.

Another important difference between treated and untreated cells is observed in surface photovoltage (SPV) measurements of CuSCN (Figure 8). A ZnO\ZnS\CdS (no LiSCN

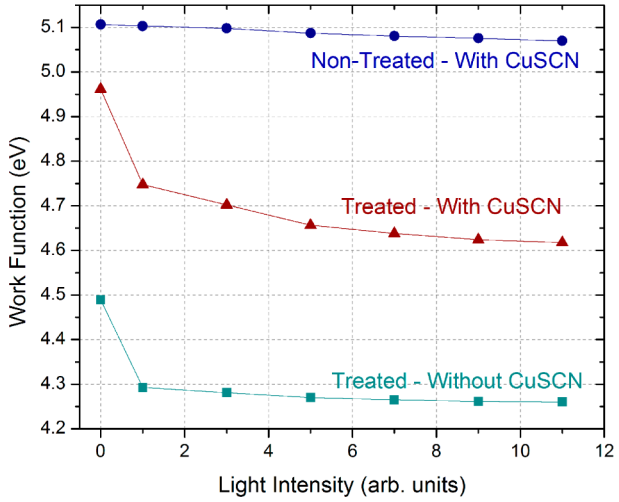

Figure 8. Kelvin probe surface photovoltage of a partial cell as a function of light intensity (ZnO\ZnS\CdS; blue−green squares); (triangles) same for a full cell with LiSCN treatment; (circles) full cell, no LiSCN treatment. Maximum light intensity is estimated as 25 mW/cm^2 (see the experimental section).

treatment) structure produces (with a cool LED source of less than 1 sun intensity) a photovoltage of ~0.23 V. The same photovoltage is obtained when the sample is dipped in LiSCN (not shown), but with a WF shift to higher values (from 4.50 to 4.85 eV). When CuSCN is deposited without prior LiSCN treatment, the photovoltage is reduced to less than 0.05 V, while with treatment, the photovoltage increases to 0.32 V. CREM-based photovoltage measurements (with a halogen light source) reveal a similar trend: with LiSCN treatment, the Cu2p signal shifts by 0.23 eV (in comparison to dark conditions) to higher E_K. Without treatment, the shift to higher E_K is <0.02 eV.

This indicates that more holes are injected into the CuSCN with the LiSCN treatment, hence the larger charging and larger shift in Cu2p. We suggest that this is a result of better electron

dx.doi.org/10.1021/am401010f | ACS Appl. Mater. Interfaces 2013, 5, 5156−5164

extraction on the CdS\ZnO side, as a result of better band alignment as described above, which results in reduction of the electron−hole recombination in the absorber.

Two additional possible contributions to the increased solar cell efficiency, as a result of the LiSCN treatment, may be suggested. First, interface states formed at the CdS\CuSCN interface (due to a chemical reaction between CdS and the CuSCN solution), may be passivated by the LiSCN treatment. Second, possible doping of the CuSCN by SCN^- should help the electrode conductance. In solution, SCN^- is a hole scavenger which upon oxidation forms a radical which reacts to form $(SCN)_3^-$ or $(SCN)_2$,[18] both of which are dopants for CuSCN. It has been shown for nanoporous TiO_2-based ETA cells that the equivalent KSCN treatment leads to doping of the CuSCN in the pores (Itzhaik et al., unpublished). In fact, we have found evidence for the importance of the cation identity, which favors the first explanation, possibly via Li^+ intercalation into one of the interfaces, but the role of the Li ion is not yet fully understood.

Employing the calculated differences in VB edges and the shifts in core levels energies upon cell construction (up to the "thin" CuSCN sample), we can draw the cell energy-band diagram.

The diagrams depicted in Figure 9 show critical differences at the bottom interface of the treated vs nontreated system. Note

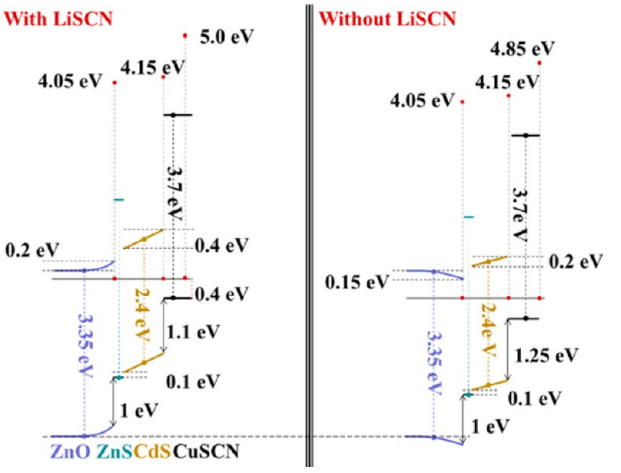

Figure 9. Energy band diagram of CdS-sensitized ETA cells. (left) With LiSCN treatment. (right) Without LiSCN treatment. The experimental error for all values is not larger than ±100 meV.

that the schemes do not account for any band bending that may exist in the bare ZnO, i.e., flat bands are assumed for the initial ZnO.

For the untreated sample, we find a small accumulation layer (or, possibly, a small decrease in depletion) that is formed between the ZnO\CdS. In the treated cells, a depletion layer evolves (larger than the one shown in Figure 9 if a depletion layer existed to begin within the ZnO). Also, we find that electric field is formed in the absorber, with magnitude that depends on the absorber thickness (a 10−15 nm thick CdS was used in these experiments).

B. Complete Solar Cells: Current Density−Voltage Results. *1. LiSCN Treatment.* *J*−*V* characteristics of cells with and without the LiSCN treatment are shown in Figure 10. The LiSCN treatment improves all the cell parameters: short circuit current (J_{sc}) from 0.8 to 1 mA/cm^2, open circuit voltage (V_{oc})

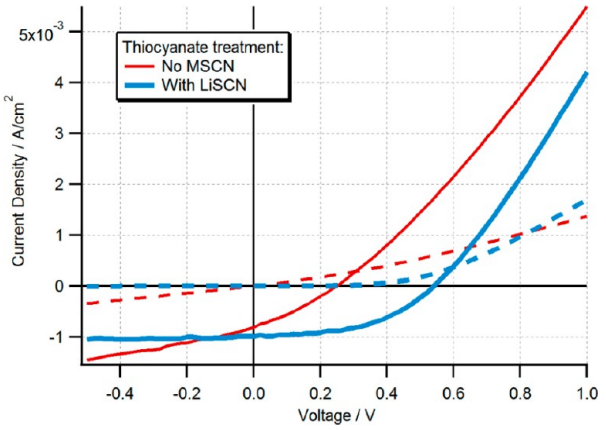

Figure 10. Current−voltage characteristics [(broken lines) dark; (solid lines) 1 sun illumination) of ETA cells with and without LiSCN treatment. Although there is a rather wide variation in the curves obtained, particularly for untreated samples, the ones shown here are typical.

from 250 to 540 mV, and fill factor (ff) from 30% to 48%. Thus, the resulting overall efficiency increases from 0.06% to 0.26%. Analysis of the dark currents reveals that the shunt resistance of cells treated with LiSCN is 2 orders of magnitude greater, and the series resistance is half as much compared with untreated cells. In addition, experiments with solar cells treated with KSCN (not shown) have shown poorer results compared with LiSCN, mainly in terms of V_{oc}. Experiments with guanidinium thiocyanate have shown even better V_{oc} but at the expense of lower currents (the magnitude of the difference was not very large—<50 mV—but not insignificant).

The photovoltage in these cells, based on Figure 9, reflects changes in the internal fields, either in the substrate and absorber (as in conventional cells, due to light-induced changes in band bending) and/or via "photodoping" at the top electrode that moves the E_F closer to the relevant energy band as in the dye sensitized solar cell. Considering first the LiSCN-treated cell, band bending in the CdS (0.4 eV) and ZnO (≥0.2 eV) gives a total possible photovoltage of ≥0.6 eV. Photodoping is expected to be negligible in the ZnO (E_F in the bulk is already close to E_C). However, there is a range up to 0.4 eV available in the CuSCN for this purpose, and indeed surface photovoltage results showed that a "half-cell" surface photovoltage (that is, without CuSCN; Figure 8) is 0.23 V, while with CuSCN it is 0.32 V, meaning that ∼0.1 V is added to the photovoltage when CuSCN is deposited, under low light intensity conditions. This makes a total potential photovoltage of >0.8 V. The V_{oc} of these (LiSCN-treated) cells vary typically between 0.5 and 0.7 V. Accepting that intense illumination and lower temperatures would increase the experimental V_{oc} further, this is still in reasonable agreement with the band diagram, particularly as it is possible that the band diagram may itself vary somewhat from cell to cell.

Additionally, the fields in both the ZnO and CdS will act to facilitate charge separation. However, the conduction band offset between CdS and ZnO is rather small, which may lead to low photocurrents (average EQE over the absorbing range typically varies between 10 and 30% although peak EQE can reach close to 50% in some cases).

For the untreated cell, there is only a small field (energy step of 0.2 eV) across the CdS to contribute to the photovoltage. Both the CuSCN and the ZnO can potentially contribute to

photovoltage through photodoping; however, our CREM data shows that, in contrast to the treated cells, there appears to be no appreciable photovoltage generated in the CuSCN. We have no direct experimental information on whether or not some photovoltage is generated in the ZnO substrate; yet the $I-V$ behavior suggests an indication for that. In terms of charge transfer dynamics, the small field created in the CdS can assist cell operation but considerably less than for the treated cell. Additionally, the probable small accumulation layer in the ZnO should act to reduce charge collection. Small fields and offsets in the conduction band are also expected to degrade the diode behavior, in agreement with the dark $I-V$ curve of the untreated cell.

2. Effect of CdS Thickness (on LiSCN-Treated Cells). The CdS thickness affects both the J_{sc} and the V_{oc} (Figure 11). In

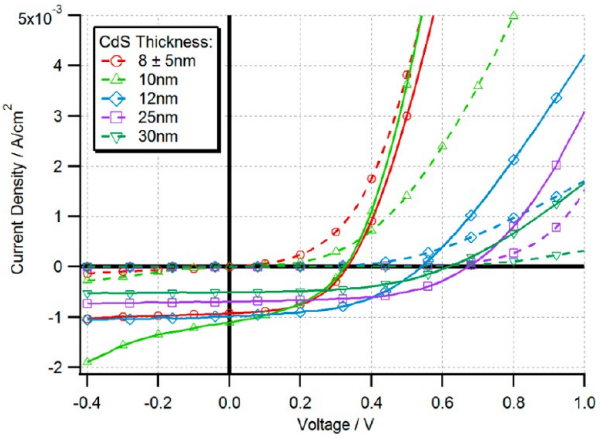

Figure 11. Current−voltage characteristics [(broken lines) dark; (solid lines) 1 sun illumination) of ETA cells with different CdS thickness (estimated values from TEM).

general, J_{sc} decreases (from 1.1 to 0.5 mA/cm^2) with increasing CdS thickness (obviously very thin CdS will give lower J_{sc} also due to low light absorption). In a field-free mechanism, such a decrease in J_{sc} with increasing CdS thickness is expected as electrons have to diffuse farther before being injected into the ZnO and thus achieve spatial separation from holes. However, we find a potential drop of 0.4 eV in the CdS that should assist charge separation. This field is seen only on initial buildup of CdS (to ca. 15 nm) and additional CdS appears to have no further effect on this value (from Figure 11, there is a significant drop in J_{sc} between 12 and 25 nm). The internal quantum efficiency does fall slightly for thin (up to at least 10 nm) films but much more rapidly for thick (20 nm) films, in agreement with the results above.

The V_{oc}, on the other hand, increases with the CdS thickness (320−670 mV) up to 25 nm and then drops. The fill factor also increases from ∼40% to ∼50%. The shunt resistance in the CdS cells shows a 2 orders of magnitude increase between 8 and 12 nm, then a more gradual increase is observed. The series resistance does not change appreciably with CdS thickness. (The cells shown in this set are typical results, but cells with open circuit voltage of up to 720 mV were obtained; the J_{sc} of these high V_{oc} cells, however, was <0.5 mA/cm^2).

Both poorer V_{oc} and fill factor are believed to result from the poorer diode behavior of a thinner CdS (breakdown at lower forward bias). One explanation for this may be that the thinner CdS does not completely cover the ZnS/ZnO (or the coverage is less than the tunneling thickness in some regions) so that recombination can occur directly at exposed ZnO/ZnS interfaces with CuSCN. This would also explain the shunting behavior of the thin CdS cells. The same V_{oc} and J_{sc} dependence on local absorber thickness was observed for ZnO\In_2S_3\CuSCN ETA cells.[19] The reasoning given in that work was that a cell with a too-thin absorber would have a significant loss route by tunneling recombination of electrons through the absorber, and this was used to explain the low V_{oc} for low absorber thickness, although it is not clear why this should reduce V_{oc} only and not J_{sc}.

3. CONCLUSIONS

The band diagram of an ZnO/ZnS/CdS/CuSCN ETA solar cell is experimentally portrayed by using XPS and CREM. It is found that there is a large VB offset (>1.1 eV) at the CdS \CuSCN interface. For comparison, 1.6 eV is expected from tabulated values. Nonetheless, this large offset translates to a large loss in V_{oc} and points at a direction to proceed in order to obtain a high V_{oc} solar cell. Also, a small conduction band offset is predicted at the ZnO\CdS interface (0.15 eV), which might explain the lower than expected currents and voltages observed in this type of cells. In total, a difference of 1.1 eV between ZnO *conduction* band and CuSCN *VB* ("effective band gap") is found, which limits the V_{oc} of these cells. Absorber-thickness dependent electric fields that increase the cell V_{oc} are found in both the oxide and the absorber, with an accumulation layer in the ZnO above certain thicknesses. A LiSCN treatment eliminates this accumulation layer, produces a depletion layer at the ZnO\CdS interface and thus improves the overall solar cell performance. This treatment also results in an increased field in the CdS that can further improve the cell.

■ ASSOCIATED CONTENT

Ⓢ Supporting Information

TEM images of ZnO/ZnS/CdS; CREM electrical loop measurements of ZnO/ZnS/CdS and of complete cells. This material is available free of charge via the Internet at http://pubs.acs.org.

■ AUTHOR INFORMATION

Corresponding Author

*E-mail: Gary.Hodes@weizmann.ac.il.

Notes

The authors declare no competing financial interest.

■ ACKNOWLEDGMENTS

E.E. is grateful to Nir Klein-Kedem for fruitful discussions. This research was supported by the Sidney E. Frank Foundation through the Israel Science Foundation (grant No. 1522/11), the Israel Ministry of Science, and Fundación Chile.

■ REFERENCES

(1) Dittrich, Th.; Belaidi, A.; Ennaoui, A. *Sol. En. Mater. Sol. Cells* **2011**, *95*, 1527−1536.
(2) Hodes, G.; Cahen, D. *Acc. Chem. Res.* **2012**, *45*, 705−713.
(3) Niles, D.; Margaritondo, G. *Phys. Rev. B: Condens. Matter Mater. Phys.* **1986**, *34*, 2923−2925.
(4) Cohen, H. *Appl. Phys. Lett.* **2004**, *85*, 1271−1273.
(5) Itzhaik, Y.; Hodes, G.; Cohen, H. *J. Phys. Chem. Lett.* **2011**, *2*, 2872−2876.
(6) Edri, E.; Rabinovich, E.; Niitsoo, O.; Cohen, H.; Bendikov, T.; Hodes, G. *J. Phys. Chem. C.* **2010**, *114*, 13092−13097.

(7) Kokotov, M.; Hodes, G. *J. Mater. Chem.* **2009**, *19*, 3847.
(8) Larramona, G.; Choné, C.; Jacob, A.; Sakakura, D.; Delatouche, B.; Péré, D.; Cieren, X.; Nagino, M.; Bayón, R. *Chem. Mater.* **2006**, *18*, 1688−1696.
(9) O'Regan, B.; Lenzmann, F.; Muis, R.; Wienke, J. *Chem. Mater.* **2002**, *14*, 5023−5029.
(10) Cohen, H.; Nogues, C.; Zon, I.; Lubomirsky, I. *J. Appl. Phys.* **2005**, *97*, 113701.
(11) Waldrop, J. R.; Grant, R. W.; Kraut, E. A. *Appl. Phys. Lett.* **1989**, *54*, 1878.
(12) Kraut, E. A.; Grant, R. W.; Waldrop, J. R.; Kowalczyk, S. P. *Phys. Rev. Lett.* **1980**, *44*, 1620−1623.
(13) Wei, S.-H.; Zunger, A. *Appl. Phys. Lett.* **1998**, *72*, 2011.
(14) Wang, Y. S.; Thomas, P. J.; O'Brien, P. *J. Phys. Chem. B.* **2006**, *110*, 21412−21415.
(15) Lahiri, J.; Batzill, M. *J. Phys. Chem. C.* **2008**, *112*, 4304−4307.
(16) Klein, A.; Säuberlich, F. *Mater. Res. Soc. Symp. Proc.* **2003**, *763*, DOI: 10.1557/PROC-763-B9.10.
(17) Säuberlich, F.; Fritsche, J.; Hunger, R.; Klein, A. *Thin Solid Films.* **2003**, *431−432*, 378−381.
(18) O'Regan, B.; Schwartz, D. T. *Chem. Mater.* **1998**, *10*, 1501−1509.
(19) Belaidi, A.; Dittrich, T.; Kieven, D.; Tornow, J.; Schwarzburg, K.; Lux-Steiner, M. *Phys. Stat. Sol. (RRL).* **2008**, *2*, 172−174.